# A High Spectral Resolution Lidar for Long-Term Unattended Operation in the Arctic

*E. W. Eloranta, R. Kuehn, R. Holz, and P. Ponsardin*
*University of Wisconsin*
*Madison, Wisconsin*

## Introduction

Global climate models suggest that the arctic climate may be particularly sensitive to perturbations caused by the increase of greenhouse gases. Arctic temperature response to a $CO_2$ doubling is predicted to be two to three times larger than the global mean.

The radiation budget of the arctic is strongly modulated by the presence of clouds. These clouds appear particularly susceptible to modification by pollution. Global circulation models have little chance of accurately predicting the arctic climate without high fidelity parameterizations describing cloud radiative properties. Current models show large variations in predicted arctic cloud cover. It is difficult to evaluate model predictions because existing arctic cloud climatologies contain large uncertainties.

The high spectral resolution lidar (HSRL) designed at the University of Wisconsin can provide vertical profiles of optical depth, backscatter cross section, depolarization, and backscatter phase function. All HSRL measurements are absolutely calibrated by reference to molecular scattering that is measured at each point in the lidar profile. This enables the HSRL to measure backscatter cross section and optical depth without a priori assumptions about the scattering properties of the atmosphere. Rigorous error estimates can be computed for all measurements. In contrast, traditional lidar measurements do not provide sufficient information to derive optical depth or scattering cross section without an assumed relationship between lidar backscatter and extinction.

Because the existing HSRL requires constant attention by a Ph.D.-level operator, it is not suited for long-term measurement campaigns. In order to overcome this restriction, the National Science Foundation (NSF) has provided funding for a new system for use in the arctic. See Table 1 for proposed system specifications. An improved optical design coupled with extensive computer control will allow unattended operation. It will be designed for easy shipment by air and will be housed in a small shelter or an existing laboratory with an up-looking window. All data and system control information will be transferred via the internet. Low-energy laser pulses will be transmitted through a large aperture such that the transmitted energy density in the output-beam is eye-safe. An avalanche photodiode detector (APD) will be used to detect the molecular backscattering instead of a photomultiplier tube. The increased quantum efficiency afforded by the APD will allow the new system to achieve measurements with a better signal-to-noise ratio than the current system. We expect to complete the system in 2001. The Atmospheric Radiation Measurement (ARM) Program's North Slope of Alaska site located at Barrow is a potential deployment site for this system.

| **Table 1**. Proposed system specifications. | |
|---|---|
| **Receiver** | |
| Aperture | 40 cm |
| Field of View | 100 μrad |
| Spectral Bandpass | 8 pm |
| Detector Quantum Eff. | ~40% |
| **Transmitter** | |
| Average Power | 0.6 W |
| Spectral Width | < 0.1 pm |
| Pulse Repetition Rate | 4 kHz |
| Beam Divergence | < 50 μrad |

# Observations

Data from the current HSRL can be used to illustrate the product expected from the new lidar. Because HSRL data analysis does not require assumptions regarding extinction-to-backscatter ratios, rigorous error limits can be computed. Figures 1, 2, and 3 show backscatter cross section, optical depth profiles, and depolarization measurements in the right panels. These profiles, which include error estimates, were derived from the cirrus cloud data shown in Figure 4. The left panels show the separate error contributions from instrument calibration errors, statistical errors in the number of photons counted, and errors in the temperature profile used to compute the molecular density. In the figures, these error terms are labeled “Calibration,” “Photon Counting,” and “Bm determination,” respectively. In order to approximate the performance of the new arctic lidar, an estimated total error curve is also shown for a system with sensitivity ten times better than the current lidar.

Recovery of optical depth and scattering cross section from traditional lidar data requires assumptions regarding the value of the scattering phase function at 180 degrees. The HSRL is able to measure this quantity directly. The HSRL determines the backscatter cross section from the ratio of aerosol scattering to molecular scattering and the extinction cross section from the rate of decrease of the molecular signal with range. In cirrus clouds, where absorption of 532-nm light is negligible, these measurements can be used to compute the backscatter phase function. Figure 5 shows a probability distribution of HSRL-measured backscatter phase functions for cirrus clouds observed over Madison, Wisconsin, during a one-year observation period. Each measurement represents a 3-min time average and a 165-m altitude average. All measurements are from altitudes greater than 3.6 km. A depolarization threshold of 20% was used to select ice clouds and eliminate liquid water clouds. Data points were selected to include only those points with an estimated backscatter cross-section error of less than 5%. An objective cloud uniformity criteria was also applied in selecting data points for this plot in order to minimize effects of multiple scattering and errors caused by averaging non-linear extinction terms. Values of the backscatter phase function derived from ray-tracing codes are shown along the top border of Figure 5. The strong peak in the measured distribution is somewhat surprising considering the wide range of values predicted by the ray-tracing codes. It appears as if the complex mixtures of crystal types observed in most clouds by in situ sampling produce a more predictable backscatter phase function than might be implied from the ray-tracing results for pristine crystals.

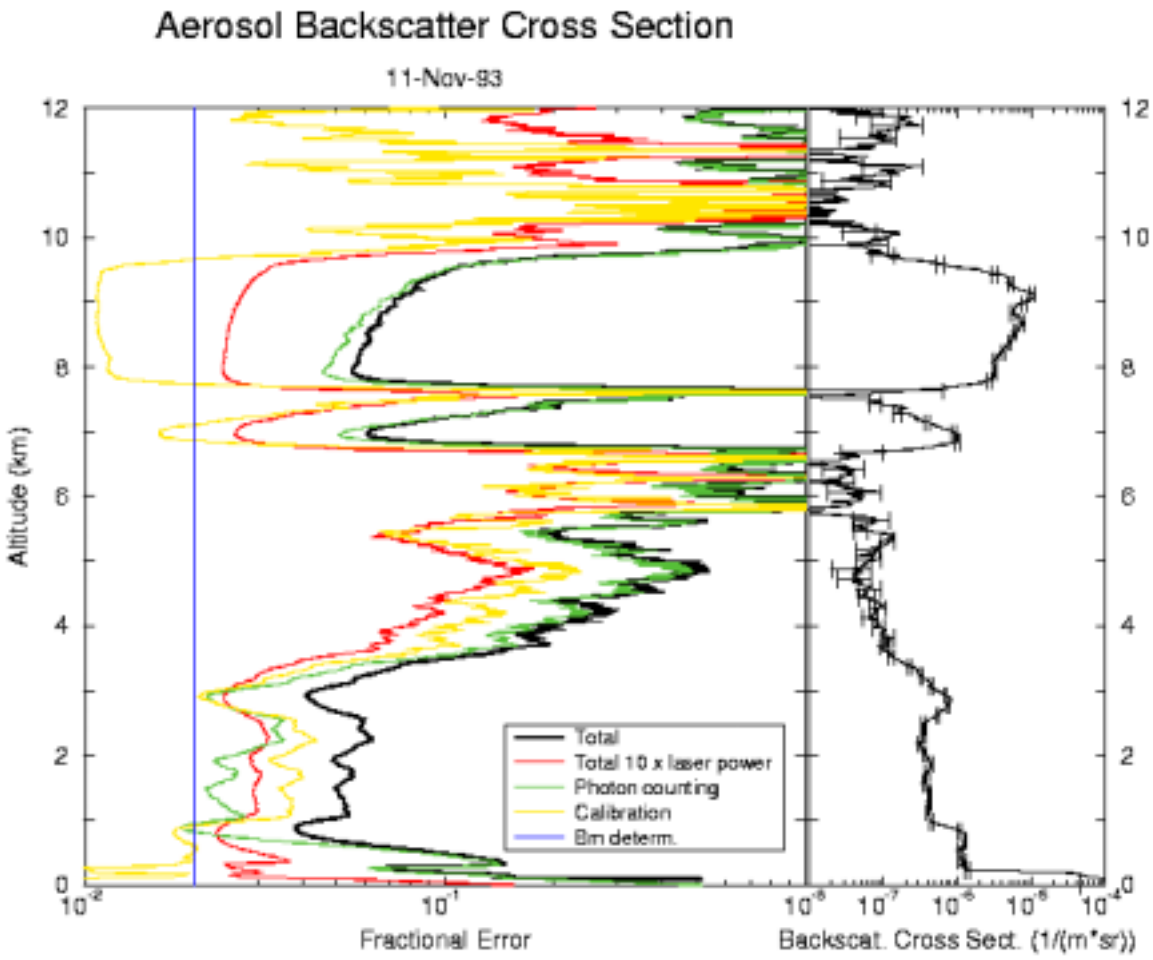


**Figure 1**. The depolarization as a function of altitude is shown on the right. The left panel shows the fractional error introduced by various sources. Notice the high depolarization produced by the non-spherical ice crystals in the cirrus cloud. Non-spherical particles are also evident in the mid-level aerosol layer between 2.5 km and 3.5 km, while scattering between 1 km and 2 km is dominated by spherical particles.

The backscatter phase function is plotted as a function of depolarization in Figure 6. It is not surprising that the backscatter phase function and the depolarization are correlated. Both factors depend on the ratio of scattering from external facets to internal reflections. For surface reflections, both the reflectivity and the depolarization are small, while internal corner reflections may provide very efficient backscattering along with high depolarization.

HSRL measurements naturally distinguish between cirrus clouds, water clouds, and aerosols. Figures 7 and 8 present the frequency of occurrence of cloud elements as a function of depolarization, temperature, and backscatter cross section. Each occurrence represents a 3-min time average and a 165-m vertical average. All data points below 15 km with an estimated error in the scattering ratio of less than

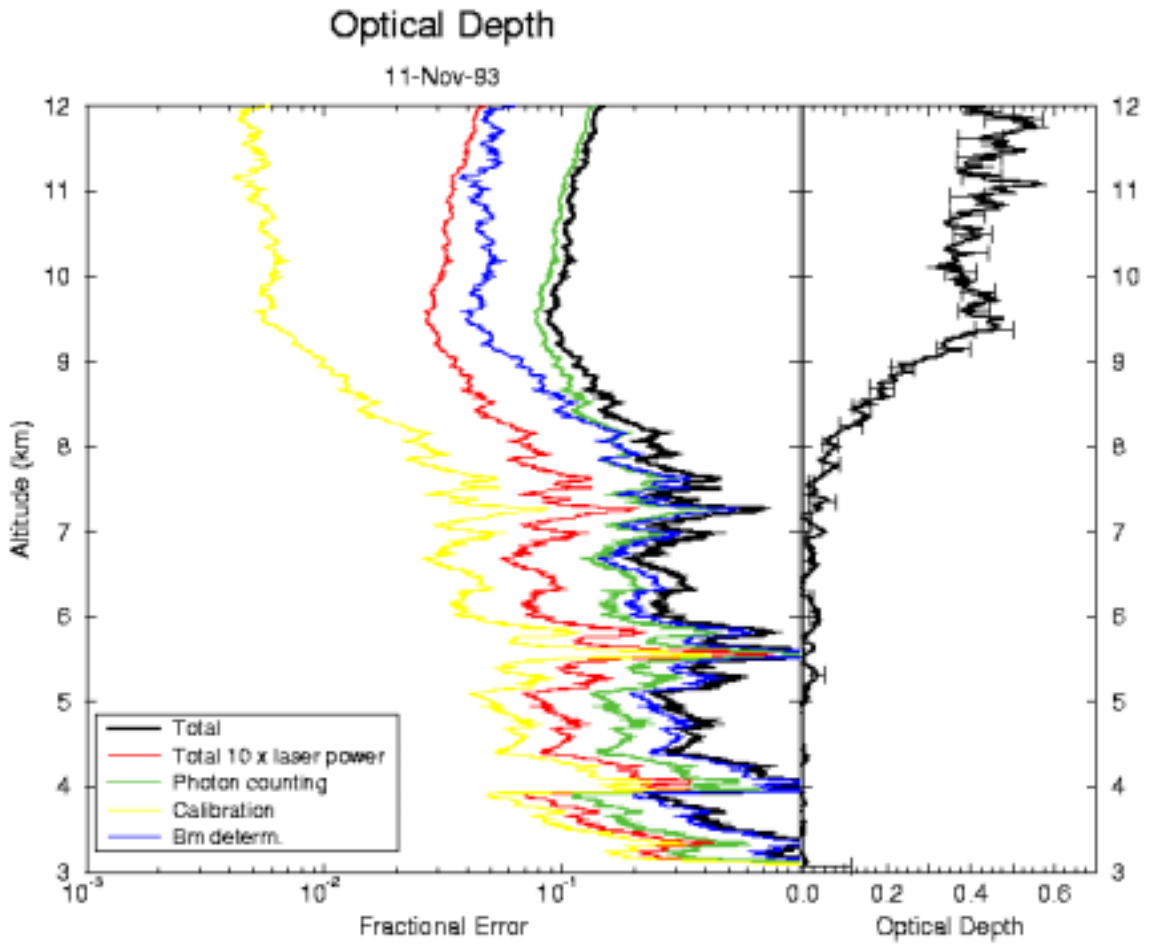


**Figure 2**. An altitude versus time plot of the calibrated backscatter cross section observed on November 11, 1993, between 1:05 Universal Time (UT) and 2:13 UT. A cirrus cloud is seen between the altitudes of 6.5 km and 10 km. Between 4 km and 5.5 km, ice crystal virga is seen falling from an altostratus water cloud near 5.5 km. Aerosol layers are visible below 3.7 km.

5% are plotted. These data were acquired as part of a cirrus cloud study and therefore, the HSRL was only operated when cirrus was present. As a result, the frequency of water clouds reported in Figure 8 is much lower than would be reported from a system that is operated continuously.

The probability distribution of optical depth for cirrus clouds observed during 1994 (Figure 9) does not show a natural limit for the minimum optical depth. This implies that definitions of cloud fraction and cloud masks are ill determined for cirrus clouds unless they are accompanied by an explicit definition of what constitutes a cloud. The fraction of the sky covered with cirrus clouds continues to increase as the cloud detection threshold is decreased.

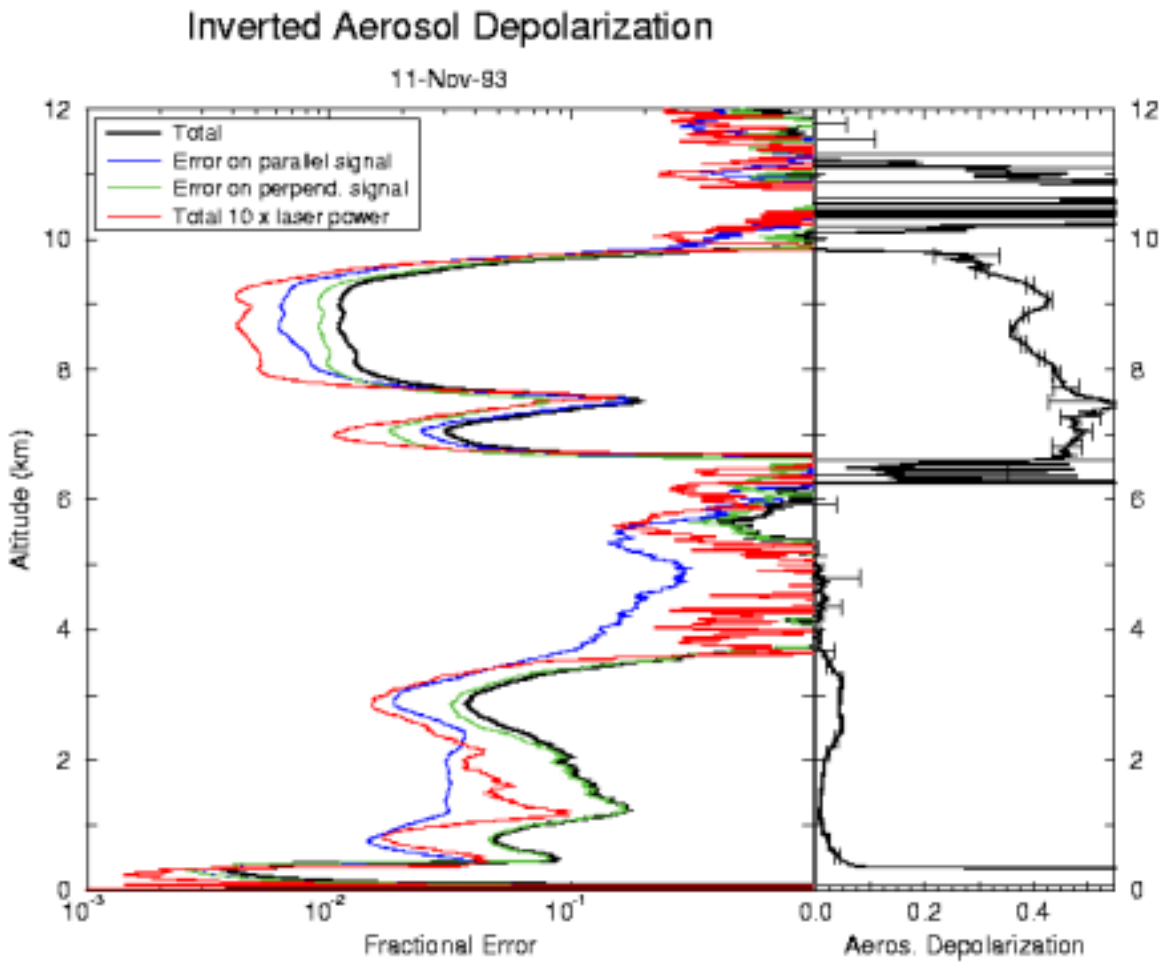


**Figure 3**. A vertical profile of aerosol backscatter cross section computed from the data shown in Figure 4 (right panel). This profile, created from data measured between 1:03 UT and 1:08 UT shows boundary layer aerosols (0 km to 1 km), mid-level aerosols (1 km to 3.7 km), and a cirrus cloud (6.5 km to 10 km). Rigorous 1-sigma error bars are plotted with the data. On the left, these errors are broken into components and plotted as fractional values. An error curve showing the effect of a ten times increase in laser power is shown to approximate the expected sensitivity increase of the new system.

## Acknowledgments

The efforts of Paivi Piironen in collecting the HSRL data are gratefully acknowledged. The arctic lidar is funded under NSF grant OPP-9910304.

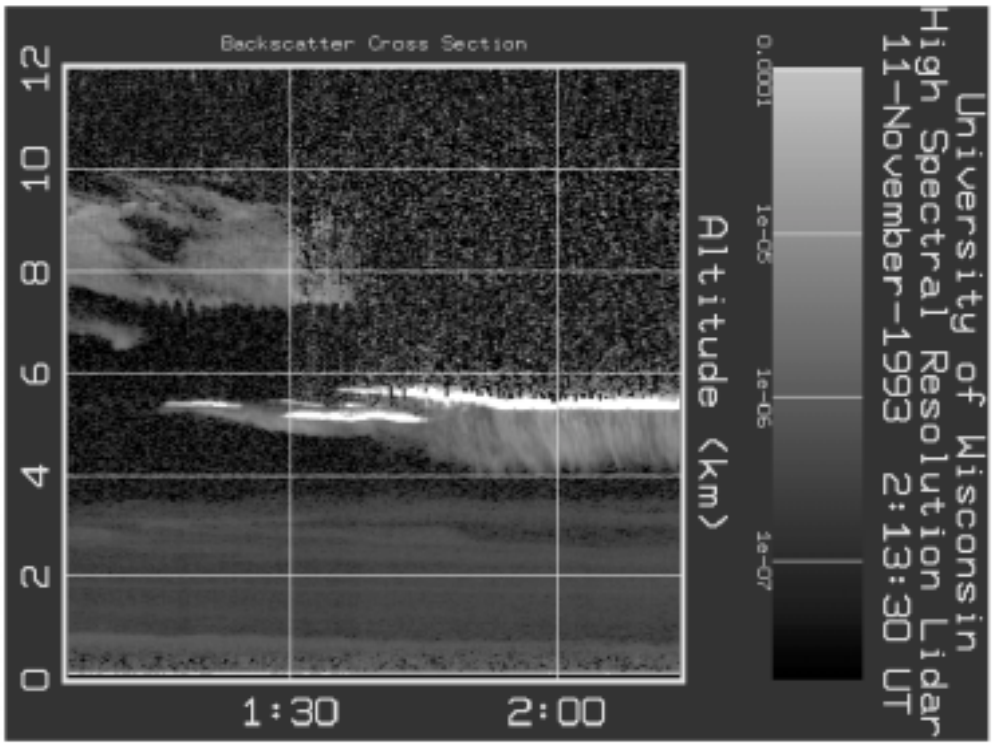


**Figure 4**. The aerosol optical depth as a function of altitude is shown on the right for the same data as in Figure 4. The left panel shows the fractional error in the optical introduced by various sources.

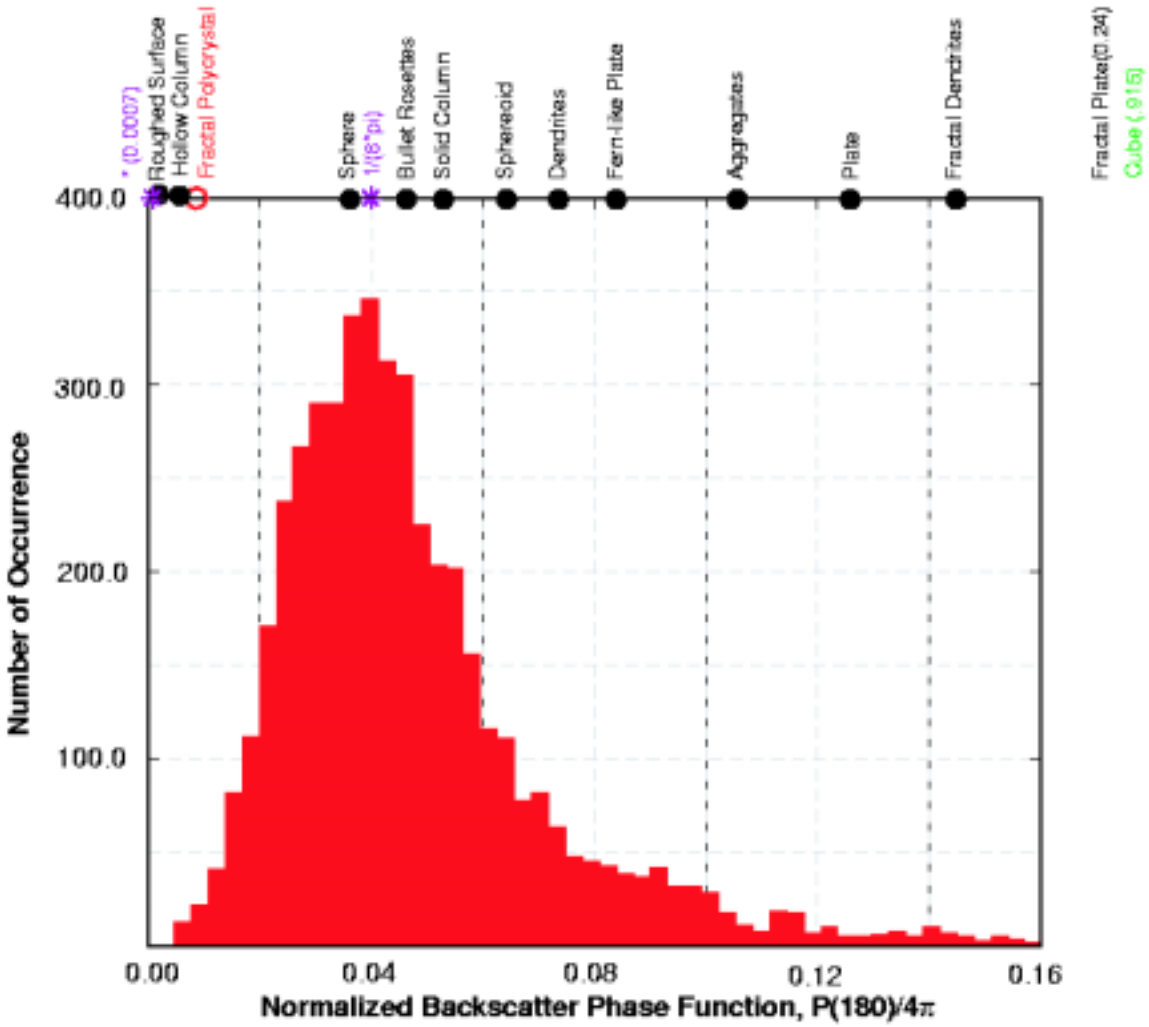


**Figure 5**. Number of occurrences of a given value of the backscatter phase function. Backscatter phase functions generated from ray tracing solutions are shown above the figure.

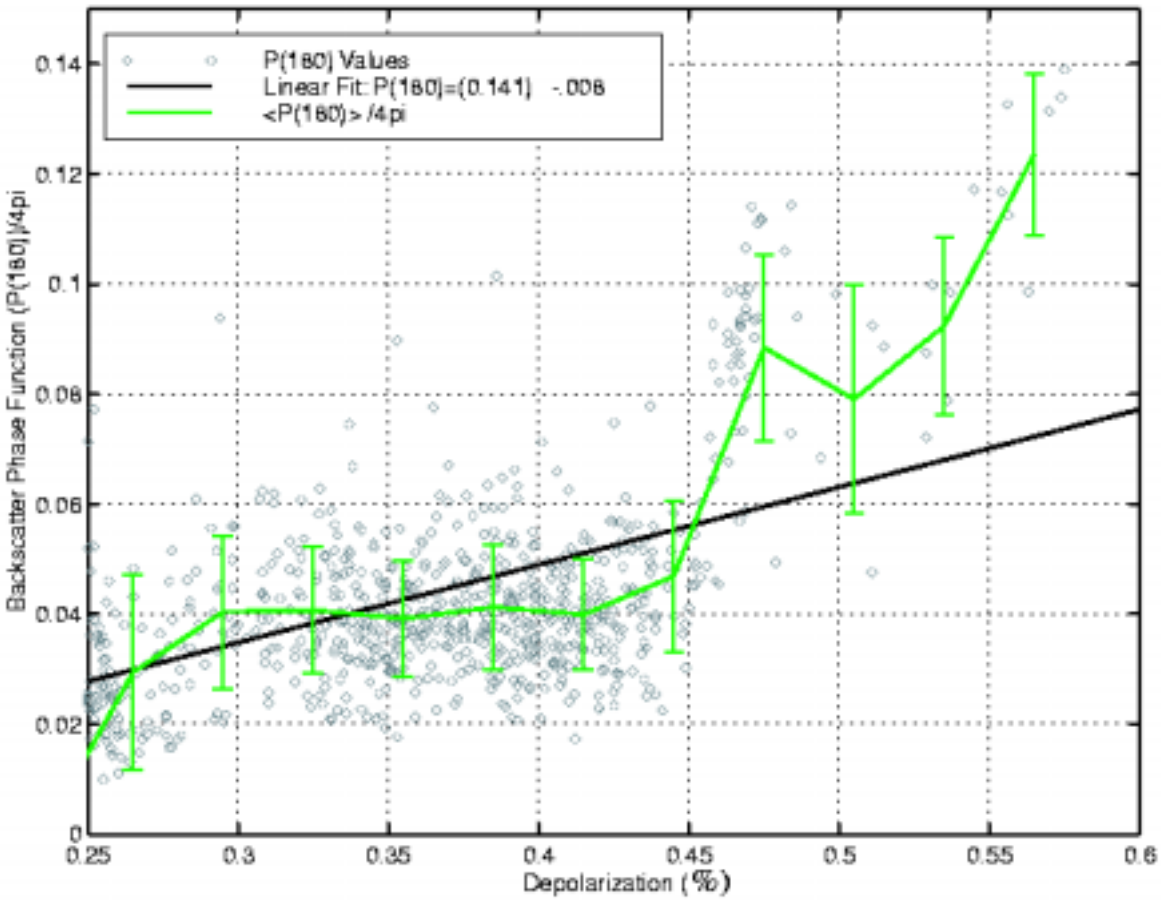


**Figure 6**. Backscatter phase function as a function of depolarization.

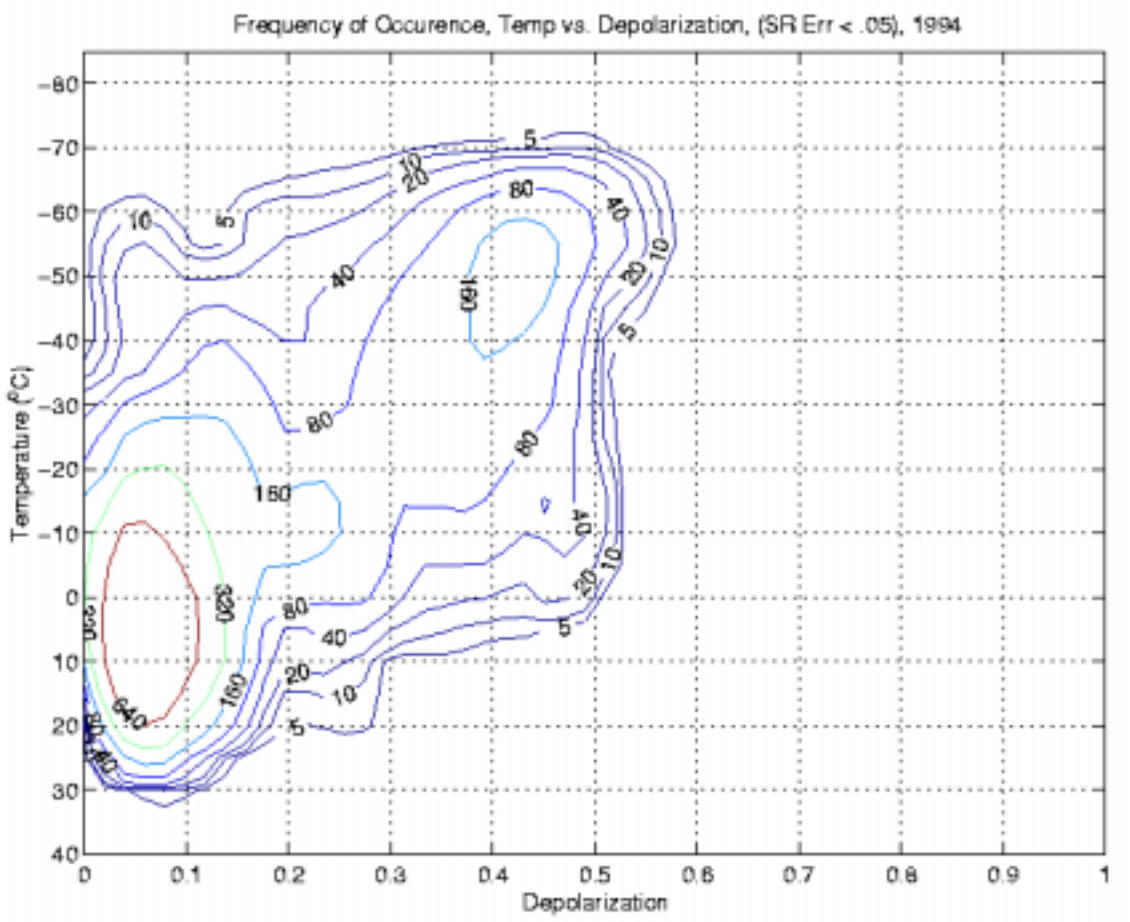


**Figure 7**. Depolarization as a function of temperature for cirrus observed during 1994. A depolarization threshold of 20% was used to select cirrus clouds. Notice the logarithmic progression of contour levels. Cirrus cloud scattering produces a maximum at a temperature of -60°C and a depolarization of 40%, while aerosol scattering produces the maximum at temperatures between -10°C and -20°C and ~6% depolarization.

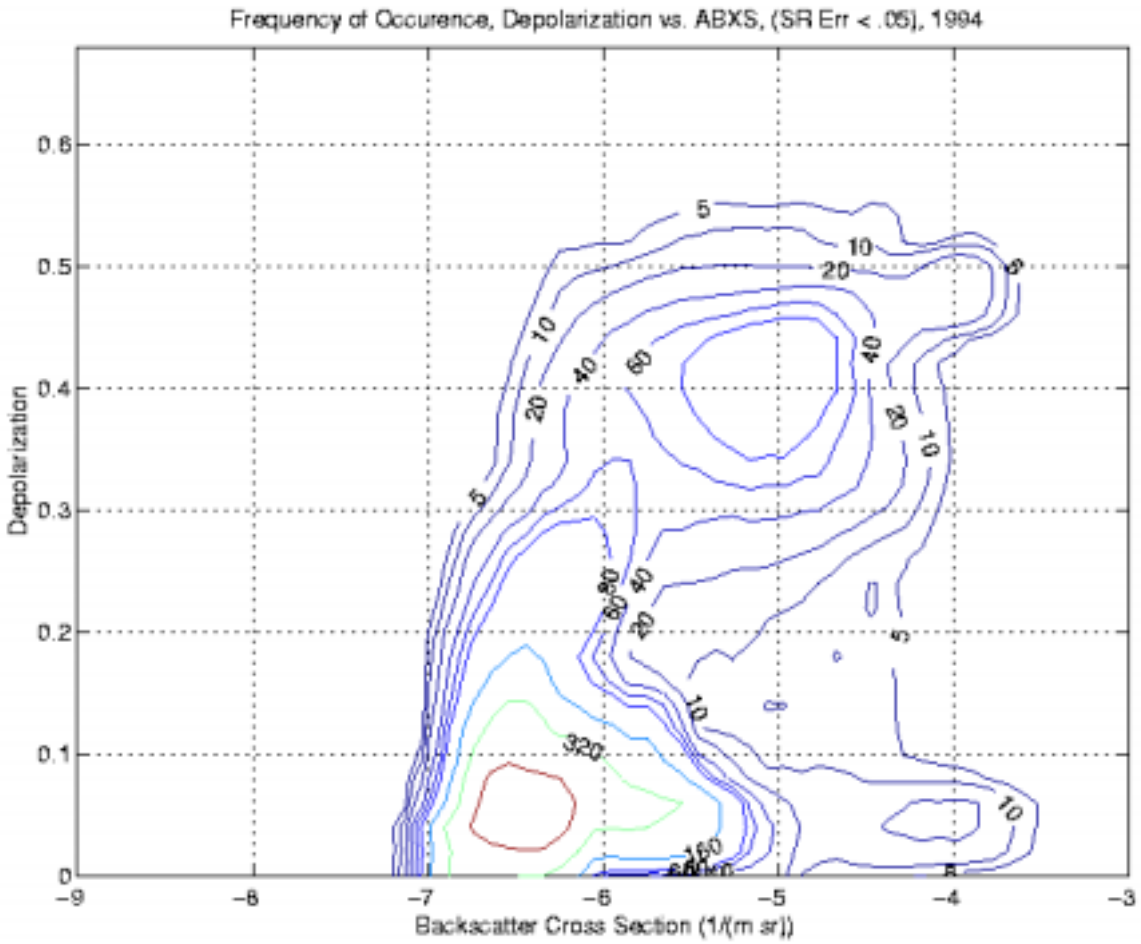


**Figure 8**. Depolarization as a function of the logarithm of the backscatter cross section. Notice the logarithmic progression of contour levels. Cirrus clouds produce the peak at a backscatter cross section of $10^{-5}m^{-1}str^{-1}$ and a depolarization of 40%, while aerosols generate the peak at $3x10^{-7}$ $m^{-1}str^{-1}$ and 6% depolarization. Water clouds generate the peak at $10^{-4}$ $m^{-1}str^{-1}$ and 4% depolarization.

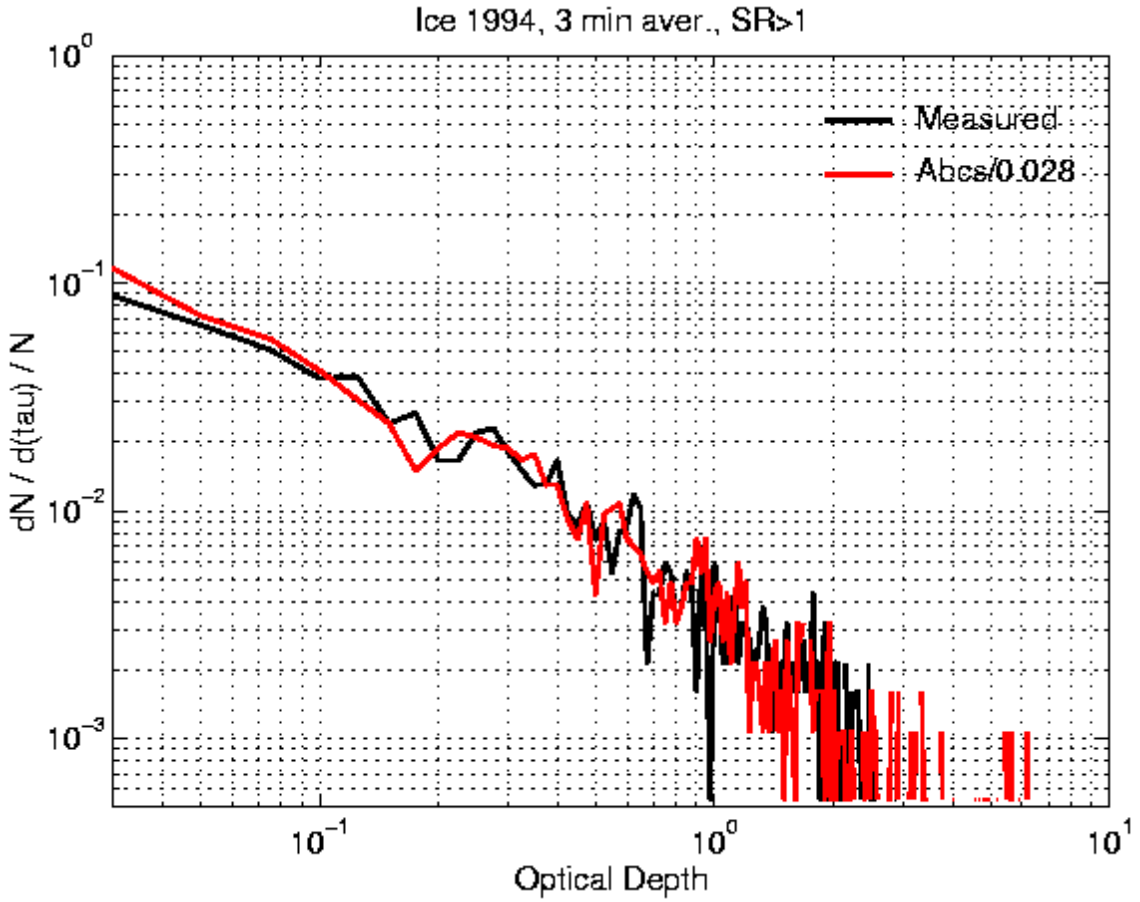


**Figure 9**. Probability distribution of optical depths for ice clouds above 3.6 km. Clouds are defined by regions where the aerosol backscatter cross section is greater than the molecular backscatter cross section. A depolarization threshold of 20% was used to distinguish between cirrus and liquid water clouds.